PAPER

Check for updates

Probing the modulation in facilitated diffusion guided by DNA–protein interactions in target search processes†

Diljith Thonnekottu [ID] [a] and Debarati Chatterjee [ID] *[ba]

Many fundamental biophysical processes involving gene regulation and gene editing rely, at the molecular level, on an intricate methodology of searching and locating the precise target base pair sequence on the genome by specific binding proteins. A unique mechanism, known as 'facilitated diffusion', which is a combination of 1D sliding along with 3D movement, is considered to be the key step for such events. This also explains the relatively much shorter timescale of the target searching process, compared to other diffusion-controlled biophysical processes. In this work, we aim to probe the modulation of target search dynamics of a protein moiety by estimating the rate of the target search process, and the statistics of the search rounds and timescales accomplished by the 1D and 3D motions, based on first passage time (FPT) calculations. This is studied with its characteristics getting influenced by various given conditions such as, when the DNA is rigid or flexible, and when the target is placed at different locations on the DNA. The current theoretical framework includes a Brownian dynamics simulation setup adopting a straightforward coarse-grained model for a diffusing protein on DNA. Moreover, this theoretical analysis provides insights into the complex target search dynamics by highlighting the significance of the chain dynamics in the mechanistic details of the facilitated diffusion process.

1 Introduction

Precise binding of a protein complex at a specific target site on the genome, out of millions of available base-pair sequences, is a salient feature governing many fundamental biophysical events such as translation, transcription, and genetic regulation.[1–10] A careful analysis into all these processes, can pinpoint a common key step, which is, finding the correct location or a specific target sequence on the DNA or genome by a protein complex while executing random movements in the cellular media. Thus, a strategy involving an efficient target search mechanism[5,11–16] governed by several non-specific as well as specific interactions finally leads to the protein binding at the target location, in spite of the random thermal movement at the molecular level. Manipulating the target search process thus obviously provides a preliminary tool to control the overall dynamics of many fundamental life processes such as genetic

regulations, protein synthesis, and many other biophysical events linked to the mechanistic details of these. Even though a large number of experimental and theoretical studies[3,8,17–35] have been performed to capture the microscopic details of this process, often, the target-searching process *in vivo* is found to be more complex. Also, the outcomes are largely guided by the modulation of the mechanistic details and the target searching process getting influenced by the specific nature of the cellular environment or media for a given condition of the concerned systems.[20,25,27,36–43] As a whole, thus, a unified description and a generalized analysis of the molecular details of target searching still remains an unresolved yet important question to address in biophysics.[12,13,25,37–40,44–47] Theoretically, the target searching events and their associated dynamics, similar to many other biophysical processes at the molecular level, can be well rationalized with a 'Reaction–Diffusion' formalism[48–50] where the reaction kinetics is governed by the slower rate-determining step, *i.e.*, the diffusive motion of the reactive species. Likewise, the target searching process, which is typically observed for transcription or gene regulation, is found to be mainly guided by diffusive dynamics at the microscopic level. However, as a simple diffusive formalism fails to capture its physically reliable fast timescale for the same, a facilitated diffusive mechanistic pathway (Fig. 1) involving 1D motion along with a 3D diffusion has been

a Department of Physics, Indian Institute of Technology Palakkad, Kerala 678623, India

b Department of Chemistry, Indian Institute of Technology Palakkad, Kerala 678623, India. E-mail: debarati@iitpkd.ac.in

† Electronic supplementary information (ESI) available. See DOI: https://doi.org/10.1039/d4cp01580k

20296 | *Phys. Chem. Chem. Phys.*, 2024, **26**, 20296–20309
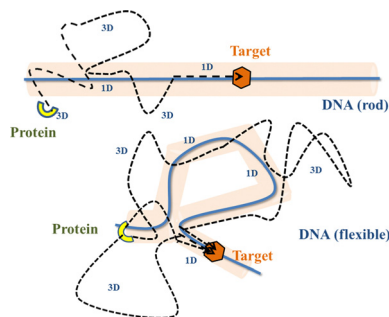
This journal is © the Owner Societies 2024

Fig. 1 Schematic representation of the current coarse-grained model. The stochastic target search trajectories of a protein complex have been depicted as a combination of 1D and 3D movements (facilitated diffusion) on a rigid, and a flexible DNA, in this figure.

theoretically conceptualized to explain the mechanism successfully.[5,11–14,24,28–30,51–56] The search strategy based on facilitated diffusion thus enables to capture the faster and more efficient target search method and hence seems to provide a reliable general technique for the target search process. Following the analytical model for the facilitated diffusion and expressing the 1D and 3D diffusion timescales with simple scaling arguments based on dimensional analysis, the target search time, τ_{tst} can be derived as,[12,57–61]

$$\tau_{tst} = N_s(\tau_{1D} + \tau_{3D}) \sim A\frac{V}{D_{3D}l_s} + B\frac{Ll_s}{D_{1D}}, \qquad (1)$$

where A, and B are geometry-related constants associated with 1D and 3D diffusion respectively, $\tau_{1D} \sim \frac{l_s^2}{D_{1D}}$ is the 1D diffusional search time, $\tau_{3D} \sim \frac{V}{D_{3D}L}$ is the 3D diffusional search time with V as the volume for the overall searched space or the cellular volume, D_{1D} and D_{3D} are the diffusion constants related to the 1D and 3D diffusive phases respectively, and $N_s = \frac{L}{l_s}$ defines the number of search rounds i.e., the number of transitions that have been made by the protein complex, from 3D to 1D phase, having L as the overall contour length of the DNA and l_s as the sliding length on DNA. The second set of expressions above simply connects τ_{tst} with other explicit and relevant parameters, revealing microscopic details, which, in turn, also provide the tools to probe the target search dynamics at the molecular level.

The recent *in vivo* study by Knight *et al.*[62] on genome interrogation by the CRISPR-Cas9 protein complex includes the mechanistic details of the target search process by the Cas9 protein complex. Motivated by the key features observed in the target search process *via* diffusion through the complex and crowded chromatin network, we suggested an exact analytical theory[63] on the basis of facilitated sub-diffusive dynamics in the context of genome interrogation and gene editing. The analytical expressions of survival probability, intensity correlation function, and mean square displacements of the protein complex which were obtained from our theory seem to agree well with the data recorded experimentally.[63] Nevertheless, it is important to note here that our previous work provides a

coarse-grained analytical model, where the target search process is investigated considering the target on a rigid rod-like DNA, which contemplates that the chain dynamics of DNA is ignored while accounting for the dynamics of the target search process, for the sake of simplicity. Recent theoretical works by Brackley *et al.*,[57,58] provide detailed Brownian dynamics simulations involving a protein modeled as a spherical particle and a target located on polymeric DNA. These studies provide a clear picture of the mechanistic details of the target search process that mimics cellular events on the microscopic length scale. Moreover, another recent study by Tyagi and Cherayil[64] provides a detailed calculation where the enhancement in the target search process has been predicted with an analytical framework based on the dynamically disordered Brownian motion of the protein, highlighting the importance of the chain dynamics synchronous with this stochastic target search event. Thus, motivated by these studies and with a view to tackling the limitations of our previous study, and also with a background of the simulation tools that have been implemented in Brackley *et al.*'s work,[57,58] we construct an MD simulation set up of the coarse-grained models for the target search process in the current work, to decode complexities in the mechanistic details, and to develop a physical intuition of the search events at the molecular level. Thus, we aim to revisit the target search process with a computational design while focusing on quantifying the dynamics at various given conditions that have been incorporated as constraints in the simulation set-up and present a comparative study at these conditions. In order to gain insights into the mechanistic details, we focus on parameters such as target search rate, 1D and 3D diffusive time scales, and the number of search rounds in each 1D or 3D phase, which were obtained directly from our simulation trajectories following the (FTP) first passage time analysis method.[65,66] Thus, implementing this analysis, the current work probes the modulation of the target search process in a quantified manner. The alteration in the characteristic features of the target search rate profiles is recorded by inducing flexibility in the polymeric backbone of DNA. The contrasting features observed in the rate profiles, accounting for the DNA chain behaving as a rigid rod or as a flexible chain, were drawn in a quantified manner. Moreover, alterations in the rate profiles were also recorded by placing the target at different locations (mainly at the end or at the center) for both rigid and flexible DNA chains. The modulation in the nature of the rate profiles, highlights the modulation in the underlying molecular dynamics of the target search process. Thus, the current study successfully captures the complex dynamical features of the target search process at the microscopic level.

In this paper, the following section on the theoretical background introduces the key equations and formal methodology to mathematically interpret the physical picture of the target searching process *via* MD simulation while also summarizing the methods to compute the target search rates for various interactions at different given conditions. The subsequent section on results provides the immediate quantified output of the theoretical framework, where we support our results with

This journal is © the Owner Societies 2024

Phys. Chem. Chem. Phys., 2024, **26**, 20296–20309 | **20297**

an analysis of various contrasting realistic scenarios. Finally, the significance of this work and future directions are presented in the Discussion and conclusions section.

2 Theoretical background

Prior to binding at the target site on a DNA molecule, the protein molecule executes a random search for the target site. As mentioned earlier, the combined dynamics involving intermittent three-dimensional (3D) bulk diffusion and one-dimensional (1D) sliding along the DNA, known as 'Facilitated Diffusion' (Fig. 1) leads to an optimal and efficient search technique which also leads to the well-suited physiological timescales for this fundamental biophysical process.[3,7,54] Here, we probe this mechanism of facilitated diffusion by a coarse-grained simulation framework and present a quantitative estimation to capture the modulation of the target search dynamics for varying target locations allied with different flexibility in the DNA backbone. The current theoretical model focuses on the target search process *via* a coarse-grained Brownian dynamics simulation set up in LAMMPS.[67] The search process of a single protein in DNA has been visualized by the diffusive search dynamics of a spherical colloidal particle for a target located on a bead-spring model of a polymeric chain as DNA (behaving either as a rigid rod or a flexible chain). In the current work, all parameters are expressed in (reduced) Lennard-Jones (LJ) units where we consider $\varepsilon = 1$, $\sigma = 1$.[68]

The time evolution of the position $\boldsymbol{q} = [x, y, z]$ of any coarse-grained particle (either a protein or a monomeric bead in DNA), is obtained by solving the Langevin equation[69-71] of the form,

$$m\ddot{\boldsymbol{q}} = -\boldsymbol{\nabla}U^{\text{int}} - \gamma\dot{\boldsymbol{q}} + \boldsymbol{\xi}(t), \qquad (2)$$

where m denotes the mass of the particle, γ is the friction coefficient, k_{B} is the Boltzmann constant, $\boldsymbol{\nabla}$ is the gradient operator, and $\boldsymbol{\xi}(t)$ is an uncorrelated Gaussian noise with first and second moments given by the following relations:

$$\langle \xi_i(t) \rangle_{\xi_i} = 0,$$
$$\langle \xi_i(t)\xi_j(t') \rangle_{\xi_i,\xi_j} = 2\gamma k_{\text{B}} T\delta(t - t')\delta_{ij}. \qquad (3)$$

where T is the temperature (T is kept constant at $T = 1$). The average $\langle \cdots \rangle_{\xi_i}$ is the average with respect to the distribution of the realizations of the stochastic variable $\xi_i(t)$. The dynamics of the protein particle is expressed with interaction potential U^{int} as $U^{\text{int}} = U^{\text{LJ}}$. The interactions between the monomeric beads of the DNA and the protein particle are represented by a truncated and shifted Lennard-Jones potential:

$$U^{\text{LJ}}(r) = \begin{cases} 4\varepsilon\left[\left(\dfrac{\sigma}{r}\right)^{12} - \left(\dfrac{\sigma}{r}\right)^{6}\right] + \varepsilon & ; r \leq r_{\text{c}} \\ 0 & ; r > r_{\text{c}} \end{cases} \qquad (4)$$

where r is the distance between the protein and the monomeric bead, and ε and σ represent the pairwise interaction energy and bead diameter, respectively. The cut-off distance $r_{\text{c}} = 2.5\sigma$ has been used in the LJ above for the interaction between DNA and

protein. In order to capture the target search dynamics for the target placed on a flexible DNA, the chain dynamics has been incorporated by the time evolution of the position of the ith monomeric beads on the DNA, which is obtained by integrating the same form of the Langevin equation (eqn (2)), but with $U^{\text{int}} = U^{\text{WCA}} + U^{\text{FENE}}$. All the monomeric beads in the DNA interact *via* a truncated and shifted Lennard-Jones potential, U^{WCA} (Weeks–Chandler–Anderson (WCA) potential) with the specific form as:

$$U^{\text{WCA}}(r) = \begin{cases} 4\varepsilon\left[\left(\dfrac{\sigma}{r}\right)^{12} - \left(\dfrac{\sigma}{r}\right)^{6}\right] + \varepsilon & ; r \leq 2^{1/6}\sigma \\ 0 & ; r > 2^{1/6}\sigma \end{cases} \qquad (5)$$

where r is the inter-particle distance and ε and σ represent the pairwise interaction energy and bead diameter, respectively. In addition, the bonded interactions between the neighboring beads in the DNA is represented by the finitely extensible nonlinear elastic (FENE) potential,[68] U^{FENE}, as follows:

$$U^{\text{FENE}}(r) = \begin{cases} -\dfrac{1}{2}kR_0^2 \ln\left[1 - \left(\dfrac{r}{R_0}\right)^2\right] & ; r < R_0 \\ \infty & ; r \geq R_0 \end{cases} \qquad (6)$$

where k is the FENE force constant and R_0 is the maximum extension of the bond. We have taken $k = 30\varepsilon/\sigma^2$ and $R_0 = 1.5\sigma$ in this study.[68] In the case of rigid DNA, in addition to the same above descriptions of the interactions for the monomeric beads, all the beads have been kept spatially fixed or immobilized to generate a rigid rod-like configuration.

As the current work focuses on probing the mechanistic details of the search technique by facilitated diffusion governed by the various interactions, this was ensured in the simulation by suitably designing specific and nonspecific interactions that closely resemble and mimic realistic biophysical events at the microscopic level. It is also important to note here that interactions between the DNA chain and the protein particle, whether specific or nonspecific, are determined by eqn (4), and remain consistent regardless of the rigid or flexible case. Thus, any such target search events start with the random movement of the coarse-grained protein particle, while the end of the event is marked by the binding at the target site on the DNA. In general, the non-specific interactions among the protein and all the monomeric beads (except the target bead) have been incorporated by $\varepsilon = \varepsilon_{\text{ns}}$ value in U^{LJ} (eqn (4)), varying from 1.0 to 8.0($k_{\text{B}}T$) in steps of 0.5($k_{\text{B}}T$) and modulation in dynamics has been estimated. However, the binding interaction or the specific interaction has been ensured in the simulation, where the interaction between only the specific target bead and protein has been kept at a much higher value, *i.e.*, $\varepsilon = \varepsilon_{\text{s}} = 100(k_{\text{B}}T)$ (eqn (4)). The relevance of this special choice of non-specific binding interaction energies, ε_{ns} and specific interaction energy, ε_{s} are explained here in detail:

(a) Non-specific interaction: by construction, this interaction, $\varepsilon_{\text{ns}} = 1$ to $8(k_{\text{B}}T)$ is acting between the coarse-grained protein particle, and all the beads on the DNA (except the target

20298 | *Phys. Chem. Chem. Phys.*, 2024, **26**, 20296–20309

This journal is © the Owner Societies 2024

bead) and is prevalent up to its LJ cut-off length, $r_c = 2.5\sigma$ (a specified radius around each DNA bead). In this study, each DNA bead has the same cut-off radius for ε_{ns}, generating a cylindrical interaction volume around the chain Fig. 3 and 4. The nonspecific interaction is designed with a range of values such that we can probe a search strategy by varying the interactions arising from all the beads, but at the same time, the interaction energy is not so high that it can perturb the essential nature of the facilitated diffusion-driven random search. For example, the non-specific interaction value should not be so high that the coarse grain particle becomes sticky to the DNA, and at the same time, it should not be so low that the particle only shows bulk diffusion. Thus, non-specific interaction is chosen to have a range of optimized values in which the modulation in the rate profiles can be captured for rigid as well as flexible DNA. Moreover, these optimized values are chosen to reproduce the target search as a facilitated diffusion process driven by a combined 1D and 3D search strategy.

(b) Specific interactions: by construction, this interaction, $\varepsilon_s = 100(k_BT)$ acts only between the target site bead and the coarse-grained protein particle and is prevalent only up to its LJ cut-off length, $r_c = 2.5\sigma$ (a specified radius around that target site bead Fig. 3 and 4). Thus, during a typical search process, if the coarse-grained particle comes inside this cutoff radius around the target site bead, it spontaneously gets driven to the target site and continues to remain close to the target bead (which is the minima of this $100k_BT$ energy well, according to the ε_s construction), indicating irreversible binding at the target site. Thus, the interaction arising from the specific target site or the specific binding energy has been kept sufficiently high (almost 10 times higher than the nonspecific interactions) to ensure, (i) the irreversible binding of the protein at the target site which is distinctly different from the nonspecific interactions, ε_{ns} and (ii) that the end of all such target search trajectories is enforced by the irreversible binding at the specific site.

Each simulation is run until the protein binds to the target bead on the DNA for the first time, and the target search time, which is determined using first passage time analysis,[65,66] and the trajectory of the protein is recorded. A time step of $\delta t = 0.001\tau$ was used in all simulations, where $\tau = (m\sigma^2/\varepsilon)^{1/2}$, and we have taken $m = 1$ for all the particles. All the post-processing of the trajectories, as well as the generation of graphical representations, have been done using Python[72] scripts. For each simulation, the protein's initial position is chosen at a random location inside the simulation box. We considered a DNA molecule of length $L = 101\sigma$, and used a rectangular simulation box ($L_x = L_y = 50\sigma$, $L_z = 150\sigma$) with periodic boundary conditions (Fig. 2). Eqn (2) is integrated numerically using the velocity-Verlet algorithm,[73] for the cases in which the DNA is either rigid or flexible.[67] We have also varied the target location from the center to one end of the DNA to see the effect of the target location on the target search dynamics. The variation of mean target search time, τ_{mtst} including the mean 1D and 3D search timescales per search round such as $\langle\tau_{1D}\rangle$, $\langle\tau_{3D}\rangle$, the profile of average number of search rounds, $\langle N_s\rangle$, and target
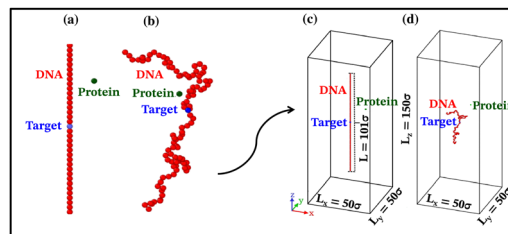

Fig. 2 A typical setup figure from the current simulation involving coarse-grained (a) rigid DNA and (b) flexible DNA, with the target (blue monomer) positioned at the center in both cases. The protein moiety (green coarse-grained bead) follows a stochastic trajectory to locate the target on the DNA. Figures (c) and (d) on the right show the simulation setups used in the current study.

search rate k, are recorded for various non-specific interaction strengths from 1000 independent simulations including rigid and flexible backbones of DNA. To characterize the 1D and 3D diffusion time scales and the number of search rounds N_s associated with each of these 1D and 3D phases from the simulation trajectory, we defined a suitable cutoff length scale. In the case of rigid DNA, we considered a cylindrical volume around the DNA having a radius of $\rho_c = 2.5\sigma$ (Fig. 3) which is practically the cut-off for the non-specific interaction. At each time, we monitored the protein's axial distance, ρ, from the DNA. If $\rho < \rho_c$, i.e. the protein is inside the cylindrical volume, we consider that the protein is executing one-dimensional diffusion, being close to the DNA backbone. On the other hand, if $\rho > \rho_c$, i.e. the protein is outside the cylindrical volume, we consider that the protein is executing three-dimensional or bulk diffusion. Similarly, in the case of a flexible DNA during the target search process, at any instant of time, if the distance of the protein from any of the beads is found to be less than $r_c = 2.5\sigma$, it is considered as 1D diffusion, being close to the DNA contour, whereas, if the distance of the protein from all of the beads is found to be more than $r_c = 2.5\sigma$, it is considered as bulk or 3D diffusion (Fig. 4). Thus, this construction of the cutoff length scale is crucial, as it allows us to characterize and
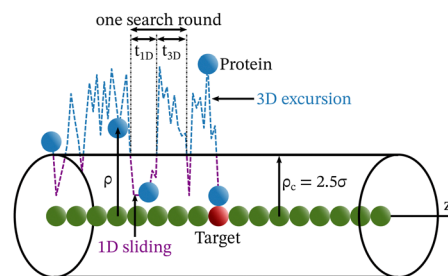

Fig. 3 Schematic diagram for the target search process by a protein complex on a rigid DNA. The same figure also depicts the method to characterize the 1D to 3D or 3D to 1D search rounds, where the 1D and 3D phases are perceived by computing the distance of the protein from the axis of the hypothetical cylinder considered, whose radius is equal to the non-specific interaction cutoff ($\rho_c = 2.5\sigma$). Thus, if the protein is inside the cylindrical volume it is considered to be in the 1D phase and if the protein is outside the cylindrical volume, it is considered to be in the bulk or 3D phase.
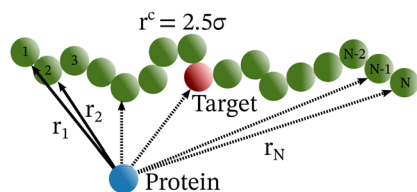
This journal is © the Owner Societies 2024

Phys. Chem. Chem. Phys., 2024, **26**, 20296–20309 | **20299**

Fig. 4 Schematic diagram of the target searching process by a protein complex on a flexible DNA. At any instant of time, if the distance of the protein from any of the beads is found to be less than $r_c = 2.5\sigma$, it is considered as 1D diffusion and if the distance of the protein from all of the beads is found to be more than $r_c = 2.5\sigma$, it is considered as bulk or 3D diffusion.
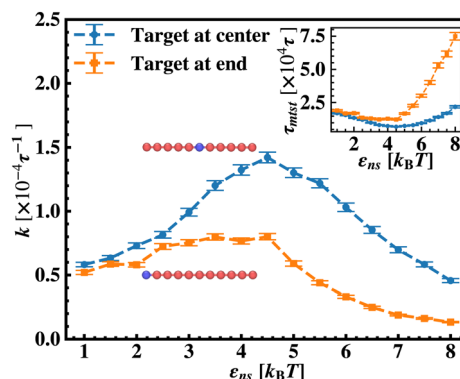

Fig. 5 Comparison of the target search rate profiles observed with the variation of the non-specific interaction strength, ε_{ns}, felt by a protein complex, diffusing on a rigid DNA when the target is kept at two different locations such as, at the center (blue '−●−', upper) and at the end (orange '−■−', lower) respectively. The inset shows the mean target search time τ_{mtst}, $\left(\tau_{mtst} = \frac{1}{k}\right)$ with the variations of ε_{ns} for the two different locations.

differentiate the 1D and 3D phases and their associated time-scales. The protein's motion between successive 1D or 3D diffusional motions has been counted as one search round. For example, if a protein executes 1D diffusion and consecutively joins to 3D diffusion and then returns to 1D diffusive phase again, that will be counted as one search round. The protein executes multiple search rounds before finding and then binding with its target. Thus, for every such whole target search run, the average time taken per search round for 1D and 3D motions were recorded along with the number of search rounds, N_s. All the measurements were computed by averaging over 1000 simulation trajectories.

3 Results

The complex dynamics of the target search process, which are regulated by a multitude of interactions, have been investigated in several prior theoretical and experimental studies[15,16,56,74] through the characterization of the target search timescale (τ_{tst}) or rate (k). Specifically, these studies indicated that increased salt concentrations shield electrostatic interactions between proteins and DNA, favoring a dominant 3D diffusion search mode, whereas, conversely, lower salt concentrations promote a 1D sliding motion of the protein along the DNA contour. This phenomenon has been replicated by adjusting the strength of non-specific interactions, ε_{ns} in this simulation framework with the coarse-grained model. This primarily, enables us to observe the impact of non-specific interactions on the 3D or 1D diffusive timescales, giving us a better understanding of the complex search dynamics in a quantified manner. Moreover, the modulation in rate profiles by manipulating these inter-actions reflects the change in the dynamical features of the target search process, highlighting the intricate characteristics of the target search process relevant to realistic biophysical scenarios.

In the current study, we analyze the dynamics of the target search process by implementing the above-described MD simulation scheme and also probe the mechanistic details of facilitated diffusion by estimating the target search rate (k) and the parameters that majorly contribute to the quantification of k, such as τ_{1D} (1D diffusive time per search round), τ_{3D} (3D diffusive time per search round), and the profile of the

number of search rounds (N_s) with the variation in the ε_{ns}. This approach also highlights the modulation in the target search dynamics for different target locations and with different flexibility in the DNA backbone and hence, provides physical insights into the mechanistic details of the target search dynamics at various given conditions at the microscopic level.

To probe into the different factors that might influence or alter the target search dynamics, firstly, we focus on the impact of different locations of the target on the DNA, as shown in Fig. 5. With a simplified coarse-grained framework of a rigid rod-like DNA, the rate of target search (k) by the diffusing protein moiety is calculated for various ε_{ns}, acting between the diffusing protein and the DNA. Considering two different target locations, such as, (a) in the middle and (b) at the end of a rigid coarse-grained conformation of DNA, the trends in the target rate profiles (k) were calculated and are depicted in Fig. 5. The overall trends in both cases remain qualitatively the same with common characteristics: (i) at the lower value of ε_{ns} ($\varepsilon_{ns} < 4.5$), k initially increases with ε_{ns}, (ii) at an inter-mediate value of ε_{ns}, k reaches a maximum, and, (iii) on further increase in the value of ε_{ns} ($\varepsilon_{ns} > 5$), k decreases. As k varies inversely to the mean target search time, *i.e.* $k = \frac{1}{\tau_{mtst}}$, k has been estimated by quantifying τ_{mtst} from the simulation trajectories. Thus the graphical representation in the inset of Fig. 5 represents the variation in the mean target search time τ_{mtst}, with the variation of ε_{ns} for two target locations on the rigid DNA. As we have mentioned earlier, following the concepts from the facilitated diffusive dynamics, the mean target search time (τ_{mtst}) is computed as,

$$\frac{1}{k} = \tau_{mtst} = \langle N_s(\tau_{1D} + \tau_{3D}) \rangle \quad (7)$$

The above equation shows that τ_{mtst} is proportional to a combination of two terms where the second term is the summation of τ_{1D}, and τ_{3D}, and the first term is the number

20300 | *Phys. Chem. Chem. Phys.*, 2024, **26**, 20296–20309

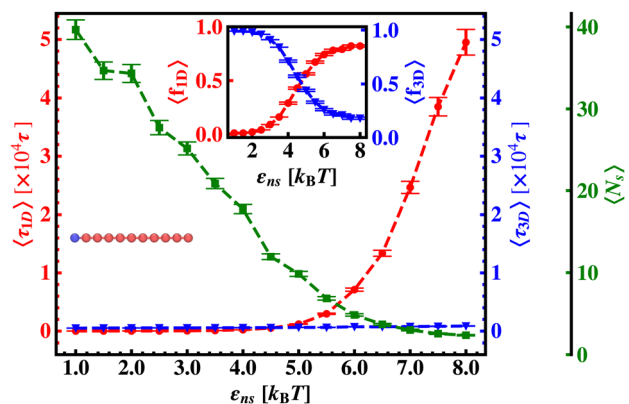This journal is © the Owner Societies 2024

Fig. 6 Variation of average one dimensional search time per search round, $\langle \tau_{1D} \rangle$ (red '–●–' line), average three dimensional search time per search round, $\langle \tau_{3D} \rangle$ (blue '–▼–' line) and the corresponding average number of search rounds, $\langle N_s \rangle$ (green '–■–' line) with non-specific interaction strength, ε_{ns}, when the target is placed at the end of a rigid DNA. The inset figure shows the variation of the average of the fractions of one dimensional search time, $\langle f_{1D} \rangle = \langle \tau_{1D}/(\tau_{1D} + \tau_{3D}) \rangle$ (red '–●–' line) and three dimensional search time, $\langle f_{3D} \rangle = \langle \tau_{3D}/(\tau_{1D} + \tau_{3D}) \rangle$ (blue '–▼–' line) with non-specific interaction strength, ε_{ns}, when the target is placed at the end of a rigid DNA.
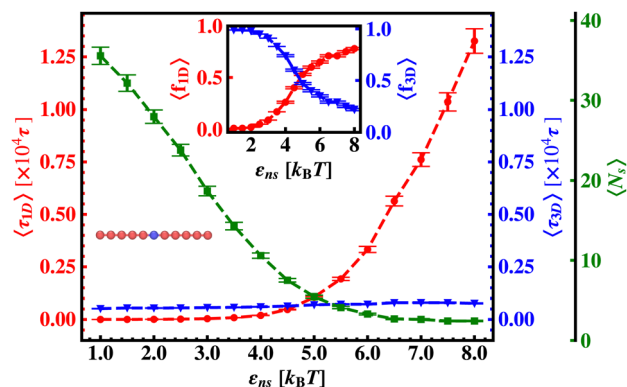
Fig. 7 Variation of average one dimensional search time per search round, $\langle \tau_{1D} \rangle$ (red '–●–' line), average three dimensional search time per search round, $\langle \tau_{3D} \rangle$ (blue '–▼–' line) and the corresponding average number of search rounds, $\langle N_s \rangle$ (green '–■–' line) with non-specific interaction strength, ε_{ns}, when the target is placed at the center of a rigid DNA. The inset figure shows the variation of the average of the fractions of one dimensional search time, $\langle f_{1D} \rangle = \langle \tau_{1D}/(\tau_{1D} + \tau_{3D}) \rangle$ (red '–●–' line) and three dimensional search time, $\langle f_{3D} \rangle = \langle \tau_{3D}/(\tau_{1D} + \tau_{3D}) \rangle$ (blue '–▼–' line) with non-specific interaction strength, ε_{ns}, when the target is placed at the center of a rigid DNA.

of rounds (N_s) associated with each of the diffusing phases of 1D or 3D. Hence, we pose a question here: how does the relative proportion of τ_{1D}, τ_{3D} and N_s get adjusted at the microscopic level at different interaction strengths to maintain an efficient search strategy for two different target locations?

Thus, next, we move on to estimate τ_{1D}, τ_{3D} and N_s from the MD simulation trajectory while varying ε_{ns} to rationalize the rate profiles obtained in the above-mentioned cases. The estimated variations of averaged τ_{1D}, τ_{3D} and N_s with ε_{ns} have been represented in Fig. 6, for the target located at the end, and in Fig. 7 for the target located in the middle of a rigid DNA, respectively. In both cases, irrespective of the two different target locations, the profiles of $\langle \tau_{1D} \rangle$, $\langle \tau_{3D} \rangle$ and $\langle N_s \rangle$ show, qualitatively, a similar trend. Thus in Fig. 6 and in Fig. 7, on increasing ε_{ns}, $\langle \tau_{1D} \rangle$ (red '–●–' line) and $\langle \tau_{3D} \rangle$ (blue '–▼–' line) the plots show overlapping trends, signifying equal contributions with similar variations up to around $\varepsilon_{ns} = 4.5$ while $\langle \tau_{1D} \rangle$ shows a monotonic increase for $\varepsilon_{ns} > 4$ and $\langle \tau_{3D} \rangle$ remains almost unaffected on further increase in the value of ε_{ns}. Additionally, $\langle N_s \rangle$ (green '–■–' line) shows a gradual decrease on increasing ε_{ns} up to $\varepsilon_{ns} = 6$ and decays to very close to 1 after a further increase in ε_{ns}. Moreover, the insets in Fig. 6 and 7 show the variation of the average of the fractions of one dimensional search time, $\langle f_{1D} \rangle = \langle \tau_{1D}/(\tau_{1D} + \tau_{3D}) \rangle$ (red '–●–' line, inset) and three dimensional search time, $\langle f_{3D} \rangle = \langle \tau_{3D}/(\tau_{1D} + \tau_{3D}) \rangle$ (blue '–▼–' line, inset) with ε_{ns}, depicting the the dominant search mode with the variation of ε_{ns} in both the cases. Thus, these graphical representations show that for the target location at the end or the middle of the rigid DNA, τ_{mtst} is dominated by $\langle N_s \rangle$ up to around $\varepsilon_{ns} = 4.5$ while, τ_{mtst} is dominated by $\langle \tau_{1D} \rangle$, in the range of $\varepsilon_{ns} > 4.5$. This justifies the trend in k in Fig. 5 as k shows an initial increase up to around $\varepsilon_{ns} = 4.5$ due to the decrease in τ_{mtst} having $\langle N_s \rangle$

(or $\langle f_{3D} \rangle$) as the determining factor that goes down sharply with the increase in ε_{ns}. Whereas, after $\varepsilon_{ns} = 4.5$, k decreases due to the increase in τ_{mtst} having $\langle \tau_{1D} \rangle$ (or $\langle f_{1D} \rangle$) as the major contributing factor governing the overall target search timescale at this range due to the monotonic increase in $\langle \tau_{1D} \rangle$ with ε_{ns}.

The significance of the above-observed trend is physically intuitive. It is important to note that, the lower values of ε_{ns} signify a weakly held diffusing protein executing a predominantly 3D bulk-diffusive search along with an intermittent 1D motion along the contour, and higher values of the ε_{ns}, on the other hand, correspond to a strongly held diffusing protein close to the DNA contour, implying a dominant 1D search. As a consequence, search dynamics with the lower ε_{ns}, is realized with intermittent 3D diffusion, which in turn enhances the overall target search rate. On the contrary, a low value of the number of search rounds is caused by higher ε_{ns}, suppressing the chances of intermittent 3D bulk diffusion, and the target search mechanism in that case is driven by the slower and rate-limiting 1D diffusing dynamics. Thus, the trend of the rate of target search with the variation in ε_{ns} in Fig. 5 probes the variation of the target search rate with a change-over in the search strategy at the microscopic level from an intermittent 1D-cum-3D diffusive motion to a predominant 1D diffusive motion. Also, it is important to note here that, the rate of target search is found to be always higher when the target is placed at the center. When the target site is spatially close to the starting position of the diffusing protein, the probability of hitting the target site by the random effects (majorly by sliding) becomes higher. This, as a whole, reflects on the higher target search rate for a protein searching for a centrally located target than the case of a target located at the end of the DNA. In addition, the observation that the rate profiles for the center and the end-
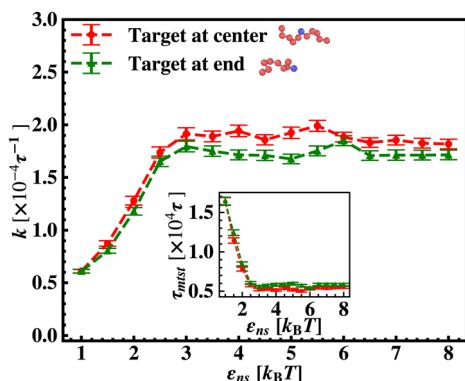
This journal is © the Owner Societies 2024

Phys. Chem. Chem. Phys., 2024, **26**, 20296–20309 | **20301**

Fig. 8 The target search rate, k, is plotted as a function of non-specific interaction strength, ε_{ns}, when the central bead is spatially fixed on a flexible DNA with the target at the center (red '−●−' line), and at one of the ends (green '−▲ −' line).

located targets are similar, indeed confirms the optimized target strategy as a combination of 3D and 1D search, (known as 'Facilitated Diffusion') irrespective of the spatial location of the target on DNA.

After these above studies, we move on to our investigations on the flexible DNA cases. Similar to the rigid DNA situation observed before, in Fig. 8, we estimate k with ε_{ns} for flexible DNA with two different placements of the targets, one at the center and the other at the end. Although the overall k profile with ε_{ns} is qualitatively different for the flexible case, the higher rate profile due to the better accessibility during the 1D motion, when the target is placed at center position is evident here as well. However, the flexibility of the backbone, allowing the intersegmental transfers or other complex search strategies involving facilitated diffusion, tends to mask the impact of the proximity effect in locating the target, unlike in the rigid DNA case. Furthermore, to analyze the rate profile with the flexible DNA case in detail, in Fig. 9 the target search rate (k) has been quantified with various interactions ε_{ns} when the target site is located at the middle of the flexible DNA
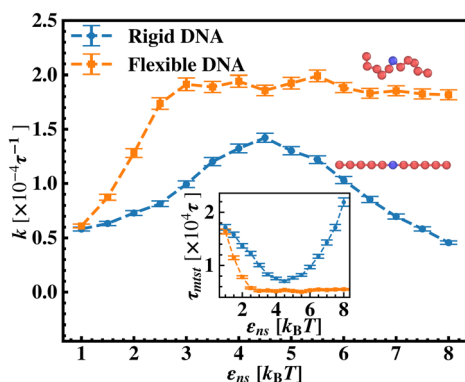
(orange '−■−' line). The rate profile for the centrally located target on a rigid DNA (blue '−●−' line) has been also shown as a function of ε_{ns} in the same graph, for the sake of comparison. The trend of k with the target on flexible DNA in Fig. 9 is found to have higher values for any ε_{ns} than that of the rigid DNA case. Hence, the graphical representation clearly indicates that k can be further manipulated to have a higher value by inducing flexibility in the DNA backbone in the same range of the ε_{ns} without altering any other system parameters. In addition, this graph also depicts that, in the initial and low range of ε_{ns}, k in both the cases, having the target on a rigid and on a flexible DNA respectively, shows an increase with ε_{ns}. In particular, for the flexible DNA case, k reaches a maximum at $\varepsilon_{ns} = 3$ while for the rigid case, k reaches a maximum at $\varepsilon_{ns} = 4.5$. Thus, the threshold value of ε_{ns} at which the maxima of k is achieved is lower for the flexible DNA case than for the rigid DNA case. Moreover, k for the flexible DNA case is found to saturate at that maximum k value even for a further increase in ε_{ns}, unlike, the case of rigid DNA where k decreases for further increase in ε_{ns} after attaining the maxima. Thus, these observations confirm that the flexibility in the backbone plays a significant role in modulating the search strategy driven by facilitated diffusion.

In continuation of our effort to probe the mechanistic details for the flexible DNA case, we estimate average τ_{1D}, τ_{3D} and N_s with ε_{ns}, involving a protein and a target placed on a flexible coarse-grained configuration of DNA in Fig. 10. Similar to what has been observed previously for a rigid DNA case, here, when the DNA has a flexible backbone, it is found that the average number of search rounds, $\langle N_s \rangle$ decreases with ε_{ns}. However, $\langle N_s \rangle$ saturates to the minimum value, *i.e.* close to 1 when $\varepsilon_{ns} = 2.5$ which clearly corresponds to a lower value of ε_{ns} than that for a rigid DNA case. Also, unlike in the rigid DNA case, $\langle \tau_{1D} \rangle$ and $\langle \tau_{3D} \rangle$ profiles no longer contribute equally at early ε_{ns} values, and apparently, they vary following two
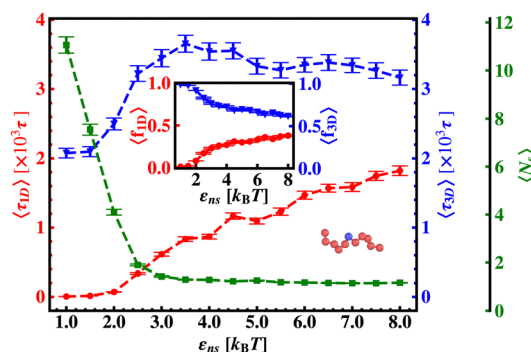

Fig. 9 Comparison of the target search rate (k) with non-specific interaction strength, ε_{ns}, for a rigid DNA (blue '−●−') and flexible DNA (orange'−■−'), when the target is placed at the center. After $\varepsilon_{ns} = 3$, unlike k for the target on a rigid DNA, k for the target on a flexible DNA, saturates at the maxima value for further increase in the ε_{ns}.

Fig. 10 The average one dimensional search time per search round, $\langle \tau_{1D} \rangle$, (red '−●−' line), the average three dimensional search time per search round, $\langle \tau_{3D} \rangle$, (blue '−▼−' line), and the corresponding average number of search rounds, $\langle N_s \rangle$ (green '−■−' dashed line) as a function of non-specific interaction strength, ε_{ns}, when the target is at the center of a flexible DNA. The inset figure shows the variation of the average of the fractions of one dimensional search time, $\langle f_{1D} \rangle = \langle \tau_{1D}/(\tau_{1D} + \tau_{3D}) \rangle$ (red '−●−' line) and three dimensional search time, $\langle f_{3D} \rangle = \langle \tau_{3D}/(\tau_{1D} + \tau_{3D}) \rangle$ (blue '−▼−' line) with non-specific interaction strength, ε_{ns}, when the target is placed at the center of a flexible DNA.

20302 | *Phys. Chem. Chem. Phys.*, 2024, **26**, 20296–20309

This journal is © the Owner Societies 2024

independent trends, with the variation of ε_{ns}. While $\langle\tau_{3D}\rangle$ saturates to a value after $\varepsilon_{ns} = 2.5$, following an initial increase, the low lying $\langle\tau_{1D}\rangle$ shows a monotonic increase with ε_{ns} in the given range of ε_{ns}. In addition, the inset of Fig. 10, shows the variation of the average of the fractions of one dimensional search time, $\langle f_{1D}\rangle = \langle\tau_{1D}/(\tau_{1D} + \tau_{3D})\rangle$ (red '–•–' line, inset) and three dimensional search time, $\langle f_{3D}\rangle = \langle\tau_{3D}/(\tau_{1D} + \tau_{3D})\rangle$ (blue '–▼–' line, inset) with ε_{ns}, depicting the the dominant search mode with the variation of ε_{ns} for the centrally located target on a flexible DNA case. It is important to note that, unlike in the case of a rigid backbone, in the case of a flexible backbone, the profile of $\langle\tau_{3D}\rangle$ makes the higher contribution to τ_{mtst}, remaining always above the $\langle\tau_{1D}\rangle$ profile and hence contributing predominantly to the measurements of k as the rate-limiting slower step. These observations also summarize that the overall target search rate (k) for a flexible backbone increases as τ_{mtst} initially decreases (with $\langle N_s\rangle$) as the most dominant term with a decreasing trend up to ($\varepsilon_{ns} = 2.5$), and then saturates to the maxima value with $\langle\tau_{3D}\rangle$ remaining as the most contributing term at the range of $\varepsilon_{ns} > 2.5$.

To further reconfirm these special characteristics of k that are attributed to the flexibility in the backbone, having originated solely from the overall chain dynamics and not from the position evolution of the target bead alone, we further look into the details of the simulation by designing three special cases to study. These are (i) the target position on the backbone is spatially fixed at a certain location, however, the other beads follow chain-dynamics (ii) the end-located bead of the flexible DNA is fixed spatially and the target bead follows the usual chain dynamics and (iii) where none of the beads including the target are spatially fixed and hence all the beads including the target beads are allowed to evolve spatially following the polymeric dynamical equation. In all three cases (Fig. 11) the nature and the trend of the rate profiles look very similar, which implies that the overall target search process is immensely impacted by a common feature *i.e.* the overall chain-dynamics in the flexible DNA case, and a similar underlying strategy for
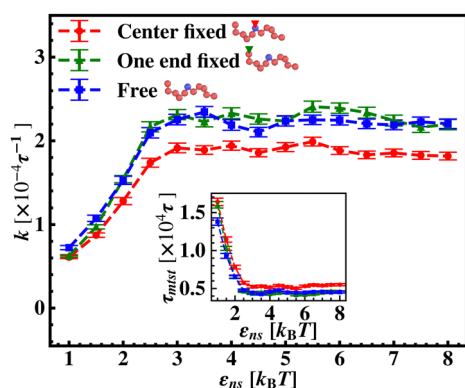

Fig. 12 The target search rate, k, is plotted as a function of non-specific interaction strength, ε_{ns}, when the target is at center and DNA is spatially fixed at center and protein is free to move (blue '–•–' line), and protein is spatially fixed and DNA is free to move (orange '–■–' line).

the target search process is operative by non-specific interactions in all these above cases.

Continuing on a similar background, we design another study to provide evidence for this unique characteristic of the target search profile arising due to the flexibility of the backbone. In Fig. 12 we compute k with ε_{ns}, obtained by conducting a comparative study in two situations where, (a) we keep only the central target bead spatially fixed, allowing the remaining beads of the DNA chain to spatially evolve as per the flexible chain dynamics and the protein particle diffuses freely and searches for the target, and (b) the coarse-grained protein particle remains spatially fixed, allowing all the DNA beads including the target to diffuse following the chain dynamics. The plots signify that the rate profile is lower when the DNA chain is allowed to evolve spatially keeping the protein particle spatially fixed, indicating the slower dynamics of the DNA chain to a protein coarse-grained particle, as expected. This study depicts the individual and explicit impact of the different relative dynamics of the protein and the DNA chain on the target search dynamics for a flexible DNA scenario, while confirming the commonality in the k profile, and hence, in the microscopic target search strategy arising due to flexibility.

Along with these quantified results, the snapshots (created using OVITO visualization software[75]) obtained from the current simulation trajectories also highlight the modulation in the mechanistic steps of the target search process at various given conditions. The snapshots obtained from our coarse-grained simulation at a specified ε_{ns} (=4.5), indicate that the target search process involving flexible DNA also shows a contrasting feature from the target search process involving rigid DNA. Thus, the time-series snapshots in Fig. 13 during the target search process involving the coarse-grained protein and flexible DNA conformation, report a dynamically evolving loop or trapped structure of the flexible chain of DNA around the protein once the protein comes close to the DNA contour unlike the target search process involving rigid DNA (Fig. 14). Moreover, these snapshots also reveal that this 1D diffusive motion of the protein along the DNA contour continues until it merges with the target, being trapped and hence evolving in

Fig. 11 The target search rate, k, is plotted as a function of non-specific interaction strength, ε_{ns}, when the target is at the center for flexible DNA (i) when the central bead (target) is spatially fixed (red '–•–' line), (ii) when one of the end beads is spatially fixed (green '–▲–' line), and (iii) none of the beads is spatially fixed (blue '–■–' dashed line).
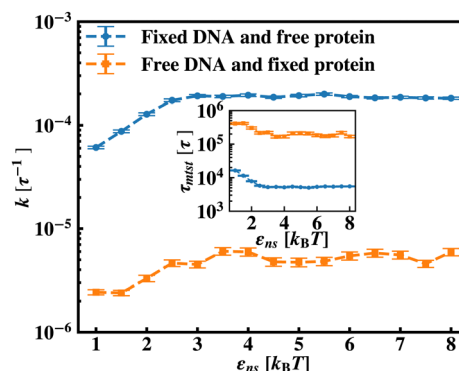
This journal is © the Owner Societies 2024

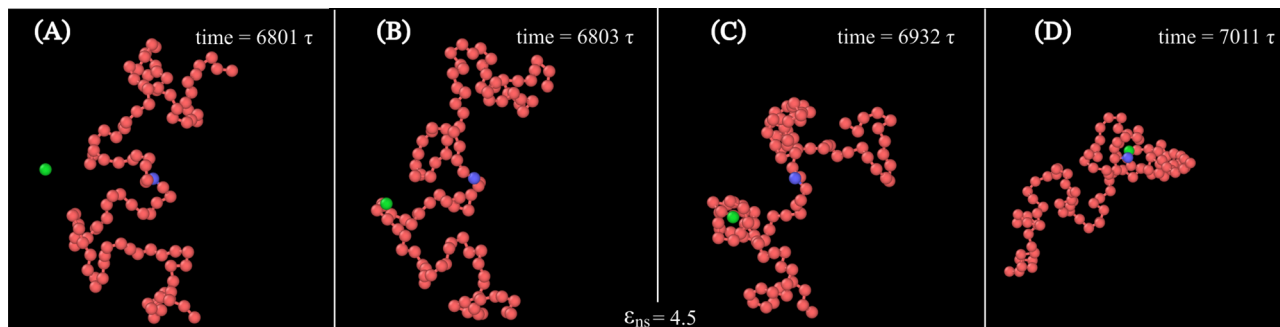*Phys. Chem. Chem. Phys.*, 2024, **26**, 20296–20309 | **20303**

Fig. 13 Time-series snapshots (A)–(D), obtained from the current simulation involving a coarse-grained protein (green spherical particle) and the target (blue bead) placed at the center of a flexible coarse-grained chain as DNA, at different instants of time.
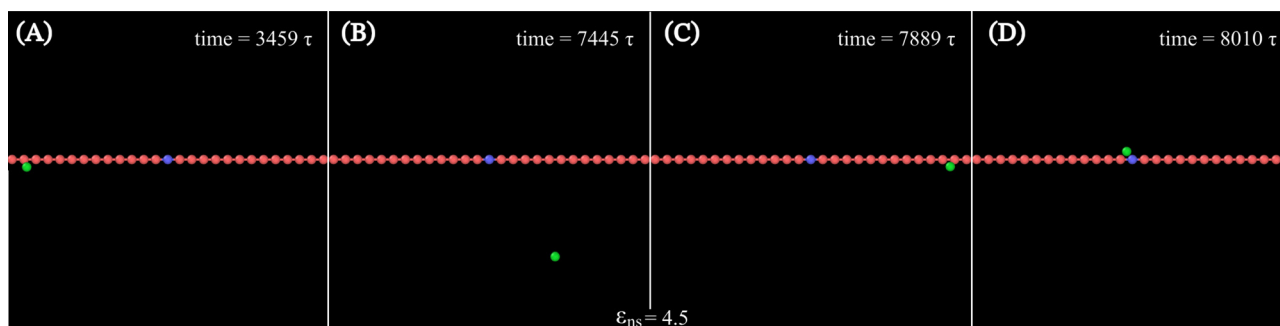

Fig. 14 Time-series snapshots (A)–(D), obtained from the current simulation involving a coarse-grained protein (green spherical particle) and the target (blue bead) placed at the center of a rigid rod-like conformation as DNA, at different instants of time.

the looped structure with the DNA backbone chain dynamics (Fig. 13).

Therefore, this investigation reveals an optimized target search strategy for each ε_{ns}, where, unlike in the case of rigid DNA where 3D diffusion is predominant only at lower values of ε_{ns} and 1D diffusion is at higher values of ε_{ns}, for the flexible DNA case, 3D diffusion prevails as a dominant feature across the entire given range of ε_{ns}. It is also noteworthy, that the 1D diffusion timescale of flexible DNA is on one hand impeded by its confinement within the looped structure of the chain, while on the other hand, when entrapped within the dynamically evolving looped structure, the 1D diffusion timescale becomes faster by intertwining with the chain dynamics and getting facilitated *via* the intersegmental transfer or other complex flexible chain property. Thus, the observed phenomenon can be explained as a dynamic disorder-driven stochastic resonance[64] amplification, specifically involving both the time-scales such as one-dimensional movement of protein and chain dynamics, simultaneously in an intricate way.

4 Discussion and conclusions

The current work presents an extensive study of the microscopic details of the target search process with a theoretical analysis based on Brownian dynamics simulation. With a straightforward coarse-grained model of a protein and a

polymeric model of DNA, the molecular insights of the target search events governed by facilitated diffusion are probed here. In reality, the molecular interaction originating due to the electrostatic interaction between the negatively charged DNA and the positively charged amino acids of proteins is the major governing factor for this facilitated diffusion-driven target search mechanism. Replicating that feature, a typical target search event has been conceptualized by the elementary event as starting with the diffusive motion driven by the non-specific interactions on the DNA chain, by the searcher protein particle, while the end of the event is marked with the binding at a specific target site placed on the DNA. In addition, following the previous relevant studies, where a dominant 3D diffusion search mode has been enhanced by shielding the electrostatic attraction at higher salt concentrations,[15,16,36,56,74] and on the other hand, the protein's 1D sliding motion along the DNA contour has been amplified by lowering salt concentrations, this probing technique has been theoretically reproduced in our coarse-grained model by manipulating the non-specific interaction strength, ε_{ns}, and monitoring the impact on the search rate k. Thus, (Fig. 6 and 7) the target search process involving the rigid DNA depicts the dominant search modes as the 3D diffusive phase at lower ε_{ns} and 1D diffusive phase, as the dominant search modes at higher ε_{ns}, which validates and remain consistent with the previous studies. To faithfully reproduce this nature the interaction between DNA beads and protein we have used, U^{LJ}, represented by Lennard-Jones

20304 | *Phys. Chem. Chem. Phys.*, 2024, **26**, 20296–20309

This journal is © the Owner Societies 2024

potential (eqn (3) and (4)), where, the ε term is characterized by two main different types of interactions, such as ε_{ns} (acting between protein and all DNA beads, except the target bead) and ε_s (acting between protein and specific target bead on DNA). This very fact signifies that ε_{ns}, even though is represented here by a short-range potential,[58] can replicate the effect of the long-range electrostatic potential,[15,16,41,56] and hence can successfully capture the essential observation and impact on the facilitated diffusion due to the electrostatic interaction. Hence by varying non-specific interactions, we manipulate the facilitated diffusion or the search mode and probe the target search event by quantifying the k profile with this ε_{ns}.

Thus, the search technique, influenced by facilitated diffusion was ensured in the simulation by suitably designing the specific and nonspecific interactions that closely resemble the physical realization and intuition at the microscopic level. Moreover, to capture the realistic details of the facilitated diffusion by identifying the 3D and 1D phases explicitly, we consider a cutoff distance from each bead on DNA (rigid, Fig. 3 or flexible, Fig. 4). This construction of the cutoff length scale, which in turn naturally follows from the specific construction of the nature of the potential, is the unique and crucial feature of the current work and hence, it can be concluded that the quantification of the search strategy obtained following this framework is a direct method to analyze the protein's motion under the effect of various nonspecific and specific interactions. This cutoff value is implemented in such a way that it can serve as a distinctive boundary between the 3D diffusive bulk phase and 1D diffusive sliding phase close to the DNA contour. In the main, therefore, this allows us to see how various interactions affect the 3D or 1D diffusive timeframe, which improves our comprehension of the intricate dynamics of the search in a quantitative way. Thus, during the search process, the location of the protein moiety and also the distance from the cutoff length, obtained from the simulation trajectory can be used to characterize the 3D or 1D diffusive phases of the protein. After characterizing the diffusive motion and its associated timescales in these two phases, the overall modulation in the rate of target search due to the change of locations of the targets was computed. Moreover, the overall

study was substantiated by carrying out a comparative analysis by considering two cases, when the target is placed on a rigid DNA and on a flexible DNA, respectively. Fig. 15 shows the graphical representations of the modulation in the $\langle N_s \rangle$ and $\langle l_S \rangle$ of the protein moiety for a rigid and flexible DNA, which have been measured separately from the simulation trajectories recalling the cutoff length scale design and the 1D diffusive motion statistics. The inverse relation of $\langle N_s \rangle$ and $\langle l_S \rangle$[58] is observed in the figure as well, confirming the robustness of the measurements and hence, once again encompassing the reliability of the current approach that has been adopted in this theoretical framework.

To capture the target search dynamics, in the current work, the dynamics of both, the coarse-grained protein particle and the beads of the DNA polymeric chain have been ensured by employing the theoretical dynamical model based on the Langevin equation (eqn (2) and (3)). Thus, it is important to note here that, even though, due to the common dynamical form in both cases, the dynamical evolution of the protein particle and the polymeric chain of DNA might appear similar (recalling the effect of individual dynamics of the protein and DNA as has been captured in Fig. 12), the relative dynamics of the protein and the monomeric beads of the DNA chain are characterized by the different form of U^{int} (eqn (4)–(6)), distinguishing the different dynamics for DNA and protein. The studies revealing the impact of the different dynamics of the protein and the DNA on the k profile, have been discussed in detail in the ESI,† available with this article, SI-A. Moreover, the average persistence length of DNA is found to be approximately 150 bp (base pairs) (in 0.1 M aqueous NaCl) and the protein binding site spans approximately 10 bp. In the current theoretical framework, where DNA is considered to be a polymeric chain consisting of 100 monomeric beads with a single bead representing the target, we can crudely map a coarse-grained quantification with the realistic situation considering each bead in the current model as equivalent to 10 bp of the realistic situation of DNA. In addition, in the current model, considering the persistence length as approximately 1 to 2 monomers, a polymeric chain consisting of 100 monomeric beads represents a fully flexible chain. Thus, comparing with the realistic
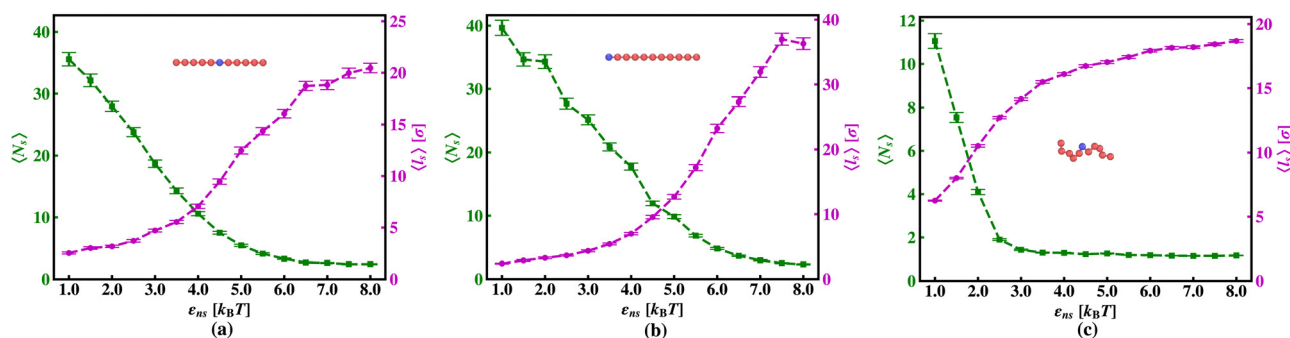

Fig. 15 The average number of search rounds, $\langle N_s \rangle$ (green '—■—' dashed line) and the average sliding length $\langle l_s \rangle$ (magenta '—●—' dashed line) as a function of non-specific interaction strength, ε_{ns}, (a) when the target is at the center of a rigid DNA, (b) when the target is at the end of a rigid DNA and, (c) when the target is at the center of a flexible DNA.

This journal is © the Owner Societies 2024

Phys. Chem. Chem. Phys., 2024, **26**, 20296–20309 | **20305**

biophysical context, we can infer that if the overall DNA length is much higher (approximately 10 times) than this 150 bp of DNA, the overall chain behaves as a fully flexible chain. On the contrary, if the overall DNA length is less then or similar to the length of 150 bp, the overall chain would behave as a rigid rod. Thus, in this current study, as we are interested in highlighting the modulation in the mechanistic details of the searcher protein for the process of target search, we have mainly focused on these two extreme situations considering when DNA is rigid and in another case where it is fully flexible. Moreover, here, the coarse-grained flexible DNA has been considered following a real Kremer–Grest polymeric chain model[68] where the persistence length is approximately equal to the diameter of individual monomeric beads, which is approximately 1σ. This ensures the fully flexible characteristics of the DNA backbone which is a deliberate choice to capture and highlight the contrasting features in the target search rate profile, concerning a rigid DNA chain. Studies of the target search rate profile including DNA as a semiflexible chain has also been touched upon in the ESI,† available with this article, SI-B.

Thus, the main inference that can be drawn from the current study is that the timescale of facilitated diffusion of the protein is altered by the additional timescale introduced by the conformational transition caused by the flexibility of the DNA chain. The current theoretical approach captures the significant molecular details of facilitated diffusion involved in the target search process, by emphasizing the effect of DNA chain flexibility on the rate of the target search process. Moreover, it is noteworthy that, the complex mechanistic features of the target search are not artificially implemented as *ad hoc* conditions in the simulation. Based on this current theoretical framework, we can recognize and characterize any complex molecular event involving these 1D and 3D phases and their associated timescales, that are central to the overall target search mechanistic steps. The statistics of the timescales in each phase are measured following the first passage analysis methods.[65,66] Here, all the characteristic search events such as hopping, sliding, or intersegmental transfers[38,56] have been visualized based on a unified description of 3D and 1D diffusive motions of the protein. Thus, in this work, a typical search trajectory involves a pure 1D (sliding), and a pure 3D (bulk) diffusion, while any other kind of complex search technique such as hopping is mapped by combining these two types (1D and 3D) of diffusive motions while intersegmental transfers are captured as a pure 1D motion, as depicted in the time series snapshots of Fig. 16. Thus, for a hopping motion which is observed for flexible as well rigid DNA, the trajectory is captured as, where the protein starts from the 1D phase near the DNA contour, then goes to 3D bulk, and subsequently again comes back to 1D phase near DNA contour, but at a different location on the DNA. The same has been explained in the schematics and snapshots, obtained from the current simulation trajectory in the representative Fig. 16 highlighting the rigid and flexible DNA scenario. Furthermore, intersegmental transfer, a unique property, owing specifically to the flexible nature of the backbone, can be defined by an event where a
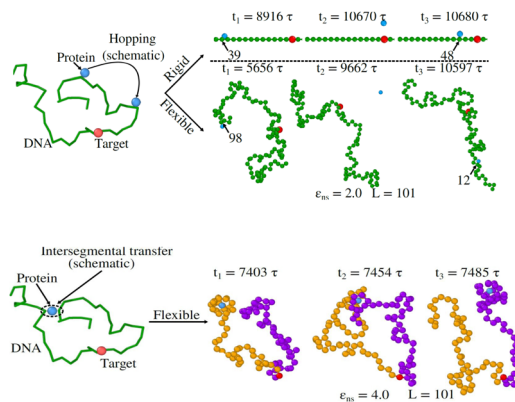

Fig. 16 (I) Upper panel: (Left) Schematic representation of hopping motion of protein (sky blue bead) on DNA (green chain) during a target (red patch) search process (Right) Simulation time series snapshots at different times showing hopping motion of a protein on a rigid DNA (first row), and on a flexible DNA (second row) of length, $L = 101$ with non-specific interaction strength, $\varepsilon_{ns} = 2.0$, (the index number of the beads of DNA) is shown to distinguish the different locations before and after hopping event. (II) Lower panel: (Left) Schematic representation of intersegmental transfer of protein (sky blue bead) between two segments of DNA (green chain) when looking for its target (red patch) (Right) Simulation time series snapshots showing intersegmental transfer of protein (sky blue bead) from segment-1 (branch with purple colored beads) to segment-2 (branch with yellow colored beads) of a flexible DNA of length, $L = 101$ with non-specific interaction strength, $\varepsilon_{ns} = 4.0$.

searcher moves from one DNA strand directly to another, which is close in space, but may be distant along the contour, by transiently binding with both. Moreover, even though it is mediated by the complex chain dynamics of the DNA chain, from the point of the searcher protein, it is just a sliding motion and is associated with its sliding timescale (τ_{1D}) along the DNA contour. Thus, in Fig. 16, we illustrate the features relevant to intersegmental transfer which is realized from the current simulation time-series snapshots.

Continuing on a similar observation as above, it can be concluded that the observations obtained from the current theory, provide a quantified prediction on how the 1D and 3D diffusion are explicitly adjusted, leading to an optimized target search strategy. The contrasting features observed in the dynamics of the search process reveal the underlying microscopic picture at various given conditions. Thus, this study identifies that with the target placed on a rigid backbone of DNA for a given variation of ε_{ns}, 1D diffusion acts as the rate-limiting step at higher ε_{ns}, while combined and intermittent 3D diffusion becomes the dominant feature at a lower ε_{ns}, which enables the protein to achieve an efficient and optimized facilitated diffusive target search strategy (Fig. 7 and 8). On the contrary, for the flexible DNA case, for the entire scanned range of ε_{ns}, 3D motion or bulk diffusion remains as the rate-limiting step and also, τ_{3D} values quickly saturate to a maximum value after initial increase with ε_{ns}. Thus, 3D motion or bulk diffusion, afterward continues to remain at that value without being affected by a further increase in the non-specific interaction strength (Fig. 10). At the same time, $\langle\tau_{1D}\rangle$ even

20306 | *Phys. Chem. Chem. Phys.*, 2024, **26**, 20296–20309

This journal is © the Owner Societies 2024

though being low lying and hence, not being the dominant phase, shows a gradual increase with ε_{ns} due to the searcher protein getting trapped by the loop-like configurations which are formed spontaneously by the flexible chain-dynamics. Hence, the 1D motion or motion along the contour for the protein, in this case, is especially noteworthy when the DNA has a flexible backbone. A stronger association between protein and DNA due to elevated ε_{ns} can lead to a more collapsed state for he DNA, hindering effective diffusion of the protein along the DNA contour. A somewhat similar logic holds for the rigid DNA case as well where a stronger association ε_{ns} between protein and DNA, due to elevated ε_{ns} leads to a better alignment of the searcher protein to the DNA contour, increasing the residing time at each bead of DNA and hence slowing down the 1D diffusion (although without the formation of any looped or trapped structure for protein), and consequently, enabling that as the dominant diffusive mode or the rate limiting phase. However, for flexible cases, despite its apparent impact as a hindrance to 1D diffusion in the looped structure, it is important to note that this collapsed state is not a static feature but is dynamically evolving with the chain dynamics, leading to events like intersegmental transfer which indirectly helps the protein moiety to reach near the target location in a faster manner, making the 1D diffusion timescale less. These two opposite effects for the flexible DNA case create differential ranges for τ_{3D} and τ_{1D} where τ_{3D} has a higher contribution being a slower timescale than τ_{1D} in the entire varied range of ε_{ns}. Thus τ_{3D} as the governing term in the target search timescale, dictates the shape of the profile of k at the higher values of ε_{ns}. This intricate interplay of flexibility and molecular interactions, as it has been visualized in the current work, have been also captured in many recent intriguing studies. The rapid long-distance migration of protein on single-stranded DNA occurring through intersegmental transfer along with multivalent interactions mediated by the flexibility of the DNA strand has been investigated with a single molecule experiment combined with a coarse-grained model in a recent study.[76] A coarse-grained molecular dynamics simulation there has been implemented to measure the size of the intersegmental transfer and the frequency of such jumps to gain insights into these complex dynamics. The interplay of electrostatic interactions and intrinsic disorder in configurational characteristics modulating target search processes has been illustrated in another recent all atom simulation study.[77] The importance of the breathing dynamics by nucleosomes has been highlighted in migrating the protein to the target site in another recent study by Mondal *et al.*[78] where it has been shown that DNA forms bulges that diffuse stochastically and may regulate the target search dynamics of a protein by nonspecifically interacting with it. Also, it is noteworthy to mention here that many other theoretical frameworks[15,35,38,41,54,79] including detailed atomistic simulations also reveals the importance of configurational characteristics of the DNA, as it has been visualized with the current theoretical framework. Thus, the significance of the current work is also in the fact that the importance of the flexibility of the DNA chain in the target search strategy,

is captured by adopting a highly coarse-grained minimal model with a Brownian dynamics simulation setup here. Thus, as our simulation snapshots depict (Fig. 13 and 14) that the protein 1D diffusion, in that case, gets synchronized with the chain dynamics, being trapped in a dynamic looped structure. With the increase in the specific strength, the protein gets trapped more effectively in the dynamic looped structure, which enhances the 1D diffusion rate of the protein by reducing the tendency to escape further in various directions and hence moves it effectively towards the target along with the loop structure as a whole, following the chain-dynamics. A similar conclusion was also made in a recent theoretical study by Tyagi and Cherayil[64] where the analytical calculation based on the Brownian motion of the protein on a flexible chain estimated an enhancement of target location rate reminiscing the phenomena of stochastic resonance. The stochastic resonance stems from the stochasticity in the conformational flexibility in the DNA along with the stochastic motion of the protein involved in the target search process. Moreover, Brackley *et al.*[57] also monitored the characteristics of the facilitated diffusion by the protein, creating the configurational trap as a static rosette-like looped structure along the flexible DNA. The facilitated diffusion of the protein with sticky interactions was captured being trapped in the loop, along the DNA flexible chain. It is important to note that the significance of the chain dynamics in the target search dynamics has been also indicated and captured *via* a different theoretical approach that includes discrete-state stochastic methods involving the master equation approach in other theoretical studies involving facilitated diffusion.[21,27,28]

Despite the fact that the current minimal coarse-grained model could effectively map the realistic nature of facilitated diffusion and can also replicate the insight into the molecular origin of the salt effect as observed in real biophysical systems, the current approach suffers from certain limitations that lead us to future avenues of exploration following a similar theoretical approach. The existing challenges from the analysis of the data could be addressed in the future by suitably modifying the current set to overcome the shortcomings and hence provide a better understanding. Primarily, the initial increase in τ_{3D} with ε_{ns} in this current work for the flexible case is puzzling and can be anticipated to originate due to the somewhat mean-field form of the potential in terms of LJ which, as a whole, wraps up information regarding any attractive or repulsive interaction from the environment and hence, in some sense captures the essential details of the electrostatic potential[36,46] in a crude way. Thus, in the future, it will be interesting to reproduce a similar computation with a more realistic potential. In addition to that, a calculation based on gradually changing the flexibility of the backbone will not only confirm the contrasting features observed in a fully flexible and rigid case but also provide the impact of the semiflexible DNA chain resembling the realistic features of DNA, with better clarity. The impact of the sequence-specific target search process will also be an interesting issue to model *via* this highly coarse-grained model based on colloidal and polymer dynamics.

This journal is © the Owner Societies 2024

Phys. Chem. Chem. Phys., 2024, **26**, 20296–20309 | **20307**

In the current theoretical model, the quantified results on the modulation in the target search rates provide an easy handle to gain a deeper insight into the process. The study is found to be suitable to provide a convenient methodology to capture the modulation in the target search rate even in a complex situation such as, in the presence of blocking agents[28,30,39,57] or in a crowded and rearranging disordered media. A natural extension of this work will be the application of a similar theoretical framework to extract testable and quantified predictions to manipulate the target search technique in a more complicated scenario.

Author contributions

Diljith Thonnekottu: investigation, visualization. Debarati Chatterjee: conceptualization, formal analysis, methodology, project administration, supervision, writing – original draft.

Data availability

The data supporting this article have been included as part of the ESI.†

Conflicts of interest

There are no conflicts to declare.

Acknowledgements

References

1 O. G. Berg, R. B. Winter and P. H. Von Hippel, *Biochemistry*, 1981, **20**, 6929–6948.
2 A. D. Riggs, S. Bourgeois and M. Cohn, *J. Mol. Biol.*, 1970, **53**, 401–417.
3 J. Elf, G.-W. Li and X. S. Xie, *Science*, 2007, **316**, 1191–1194.
4 P. H. von Hippel, *Annu. Rev. Biophys. Biomol. Struct.*, 2007, **36**, 79–105.
5 L. Mirny, M. Slutsky, Z. Wunderlich, A. Tafvizi, J. Leith and A. Kosmrlj, *J. Phys. A: Math. Theor.*, 2009, **42**, 434013.
6 A. Tafvizi, L. A. Mirny and A. M. van Oijen, *ChemPhysChem*, 2011, **12**, 1481–1489.
7 J. Yu, J. Xiao, X. Ren, K. Lao and X. S. Xie, *Science*, 2006, **311**, 1600–1603.
8 R. B. Winter and P. H. Von Hippel, *Biochemistry*, 1981, **20**, 6948–6960.
9 G. Kolesov, Z. Wunderlich, O. N. Laikova, M. S. Gelfand and L. A. Mirny, *Proc. Natl. Acad. Sci U. S. A.*, 2007, **104**, 13948–13953.
10 M. Woringer, X. Darzacq and I. Izeddin, *Curr. Opin. Chem. Biol.*, 2014, **20**, 112–119.
11 P. H. von Hippel and O. G. Berg, *J. Biol. Chem.*, 1989, **264**, 675–678.
12 A. B. Kolomeisky, *Phys. Chem. Chem. Phys.*, 2011, **13**, 2088–2095.
13 A. A. Shvets, M. P. Kochugaeva and A. B. Kolomeisky, *Molecules*, 2018, **23**, 2106.
14 Z. Wunderlich and L. A. Mirny, *Nucleic Acids Res.*, 2008, **36**, 3570–3578.
15 A. Bhattacherjee and Y. Levy, *Nucleic Acids Res.*, 2014, **42**, 12404–12414.
16 A. Bhattacherjee and Y. Levy, *Nucleic Acids Res.*, 2014, **42**, 12415–12424.
17 A. J. Pollak, A. T. Chin and N. O. Reich, *Biochemistry*, 2014, **53**, 7028–7037.
18 P. Hammar, P. Leroy, A. Mahmutovic, E. G. Marklund, O. G. Berg and J. Elf, *Science*, 2012, **336**, 1595–1598.
19 Y. Wang, R. H. Austin and E. C. Cox, *Phys. Rev. Lett.*, 2006, **97**, 048302.
20 J. Gorman, A. J. Plys, M.-L. Visnapuu, E. Alani and E. C. Greene, *Nat. Struct. Mol. Biol.*, 2010, **17**, 932–938.
21 J. Iwahara and A. B. Kolomeisky, *Biophys. Chem.*, 2021, **269**, 106521.
22 I. Izeddin, V. Récamier, L. Bosanac, I. I. Cissé, L. Boudarene, C. Dugast-Darzacq, F. Proux, O. Bénichou, R. Voituriez and O. Bensaude, *et al.*, *eLife*, 2014, **3**, e02230.
23 V. Dahirel, F. Paillusson, M. Jardat, M. Barbi and J.-M. Victor, *Phys. Rev. Lett.*, 2009, **102**, 228101.
24 L. Liu, A. G. Cherstvy and R. Metzler, *J. Phys. Chem. B*, 2017, **121**, 1284–1289.
25 E. F. Koslover, M. A. D. de la Rosa and A. J. Spakowitz, *Biophys. J.*, 2011, **101**, 856–865.
26 T. Ando and J. Skolnick, *PLoS Comput. Biol.*, 2014, **10**, e1003990.
27 C. Felipe, J. Shin and A. B. Kolomeisky, *J. Phys. Chem. B*, 2021, **125**, 1727–1734.
28 C. Felipe, J. Shin, Y. Loginova and A. B. Kolomeisky, *J. Chem. Phys.*, 2020, **152**, 025101.
29 K. Mondal and S. Chaudhury, *J. Stat. Mech.: Theory Exp.*, 2020, **2020**, 093204.
30 B. Punia and S. Chaudhury, *J. Phys. Chem. B*, 2022, **126**, 3037–3047.
31 D. Normanno, L. Boudarène, C. Dugast-Darzacq, J. Chen, C. Richter, F. Proux, O. Bénichou, R. Voituriez, X. Darzacq and M. Dahan, *Nat. Commun.*, 2015, **6**, 7357.
32 A. S. Hansen, A. Amitai, C. Cattoglio, R. Tjian and X. Darzacq, *Nat. Chem. Biol.*, 2020, **16**, 257–266.
33 T. E. Kuhlman and E. C. Cox, *Mol. Syst. Biol.*, 2012, **8**, 610.
34 N. Hao, K. E. Shearwin and I. B. Dodd, *Nat. Commun.*, 2017, **8**, 1628.
35 D. Vuzman and Y. Levy, *Proc. Natl. Acad. Sci U. S. A.*, 2010, **107**, 21004–21009.

36 Y. Levy, J. N. Onuchic and P. G. Wolynes, *J. Am. Chem. Soc.*, 2007, **129**, 738–739.

37 B. van den Broek, M. A. Lomholt, S.-M. Kalisch, R. Metzler and G. J. Wuite, *Proc. Natl. Acad. Sci U. S. A.*, 2008, **105**, 15738–15742.

38 A. Mondal and A. Bhattacherjee, *Nucleic Acids Res.*, 2015, **43**, 9176–9186.

39 P. Dey and A. Bhattacherjee, *Soft Matter*, 2019, **15**, 1960–1969.

40 O. Pulkkinen and R. Metzler, *Phys. Rev. Lett.*, 2013, **110**, 198101.

41 A. Marcovitz and Y. Levy, *Proc. Natl. Acad. Sci. U. S. A.*, 2011, **108**, 17957–17962.

42 G.-W. Li, O. G. Berg and J. Elf, *Nat. Phys.*, 2009, **5**, 294–297.

43 L. Liu and K. Luo, *J. Chem. Phys.*, 2015, **142**, 03B613_1.

44 S. E. Halford, *Biochem. Soc. Trans.*, 2009, **37**, 343–348.

45 A. Cherstvy, A. Kolomeisky and A. Kornyshev, *J. Phys. Chem. B*, 2008, **112**, 4741–4750.

46 L. S. Bigman, H. M. Greenblatt and Y. Levy, *J. Phys. Chem. B*, 2021, **125**, 3119–3131.

47 A. Veksler and A. B. Kolomeisky, *J. Phys. Chem. B*, 2013, **117**, 12695–12701.

48 O. Bénichou, M. Moreau and G. Oshanin, *Phys. Rev. E: Stat., Nonlinear, Soft Matter Phys.*, 2000, **61**, 3388.

49 D. Shoup, G. Lipari and A. Szabo, *Biophys. J.*, 1981, **36**, 697–714.

50 S. Park, O.-C. Lee, X. Durang and J.-H. Jeon, *J. Korean Phys. Soc.*, 2021, **78**, 408–426.

51 C. Bustamante, M. Guthold, X. Zhu and G. Yang, *J. Biol. Chem.*, 1999, **274**, 16665–16668.

52 C. Loverdo, O. Benichou, R. Voituriez, A. Biebricher, I. Bonnet and P. Desbiolles, *Phys. Rev. Lett.*, 2009, **102**, 188101.

53 R. K. Das and A. B. Kolomeisky, *Phys. Chem. Chem. Phys.*, 2010, **12**, 2999–3004.

54 P. Kar, A. G. Cherstvy and R. Metzler, *Phys. Chem. Chem. Phys.*, 2018, **20**, 7931–7946.

55 E. Chow and J. Skolnick, *Biophys. J.*, 2017, **112**, 2261–2270.

56 O. Givaty and Y. Levy, *J. Mol. Biol.*, 2009, **385**, 1087–1097.

57 C. A. Brackley, M. E. Cates and D. Marenduzzo, *Phys. Rev. Lett.*, 2013, **111**, 108101.

58 C. A. Brackley, M. E. Cates and D. Marenduzzo, *Phys. Rev. Lett.*, 2012, **109**, 168103.

59 M. B. Elowitz, M. G. Surette, P.-E. Wolf, J. B. Stock and S. Leibler, *J. Bacteriol.*, 1999, **181**, 197–203.

60 O. Bénichou, Y. Kafri, M. Sheinman and R. Voituriez, *Phys. Rev. Lett.*, 2009, **103**, 138102.

61 S. E. Halford and J. F. Marko, *Nucleic Acids Res.*, 2004, **32**, 3040–3052.

62 S. C. Knight, L. Xie, W. Deng, B. Guglielmi, L. B. Witkowsky, L. Bosanac, E. T. Zhang, M. El Beheiry, J.-B. Masson and M. Dahan, *et al.*, *Science*, 2015, **350**, 823–826.

63 D. Thonnekottu and D. Chatterjee, *J. Phys. Chem. B*, 2020, **124**, 3271–3282.

64 N. Tyagi and B. J. Cherayil, *J. Stat. Mech.: Theory Exp.*, 2018, **2018**, 063208.

65 S. Redner, *A Guide to First-Passage Processes*, Cambridge University Press, 2001.

66 R. Metzler, S. Redner and G. Oshanin, *First-passage Phenomena And Their Applications*, World Scientific, 2014, vol. 35.

67 A. P. Thompson, H. M. Aktulga, R. Berger, D. S. Bolintineanu, W. M. Brown, P. S. Crozier, P. J. in't Veld, A. Kohlmeyer, S. G. Moore and T. D. Nguyen, *et al.*, LAMMPS-a flexible simulation tool for particle-based materials modeling at the atomic, meso, and continuum scales, *Comput. Phys. Commun.*, 2022, **271**, 108171.

68 K. Kremer and G. S. Grest, *J. Chem. Phys.*, 1990, **92**, 5057–5086.

69 R. Zwanzig, *Nonequilibrium Statistical Mechanics*, Oxford University Press, 2001.

70 C. W. Gardiner, *Handbook of Stochastic Methods for Physics, Chemistry and the Natural Sciences*, Springer, Berlin, 1983.

71 D. A. McQuarrie, *Statistical Mechanics*, Harper & Row, New York, 1976.

72 G. van Rossum and J. de Boer, *Interactively Testing Remote Servers Using the Python Programming Language*, 1991, **4**, pp. 283–304, **https://www.python.org**.

73 L. Verlet, *Phys. Rev.*, 1967, **159**, 98.

74 S. C. Piatt, J. J. Loparo and A. C. Price, *Biophys. J.*, 2019, **116**, 2367–2377.

75 A. Stukowski, Visualization and analysis of atomistic simulation data with OVITO-the Open Visualization Tool, *Modell. Simul. Mater. Sci. Eng.*, 2010, **18**, 015012.

76 S. Pangeni, G. Biswas, V. Kaushik, S. Kuppa, O. Yang, C.-T. Lin, G. Mishra, Y. Levy, E. Antony and T. Ha, *J. Mol. Biol.*, 2024, **436**, 168491.

77 L. S. Bigman and Y. Levy, *Annu. Rev. Biophys.*, 2023, **52**, 463–486.

78 A. Mondal, S. K. Mishra and A. Bhattacherjee, *Biophys. J.*, 2022, **121**, 4526–4542.

79 G. Naiya, P. Raha, M. K. Mondal, U. Pal, R. Saha, S. Chaudhuri, S. Batabyal, S. Kumar Pal, D. Bhattacharyya, N. C. Maiti and S. Roy, *Phys. Chem. Chem. Phys.*, 2016, **18**, 21618–21628.

This journal is © the Owner Societies 2024

Phys. Chem. Chem. Phys., 2024, **26**, 20296–20309 | **20309**